IEEE Access
Multidisciplinary : Rapid Review : Open Access Journal

Received 23 April 2022, accepted 11 May 2022, date of publication 17 May 2022, date of current version 25 August 2022.

Digital Object Identifier 10.1109/ACCESS.2022.3175788

RESEARCH ARTICLE

Boundaryless Visible Light Communication System Without Attocell for Industrial Internet of Things

JING-SHU XUE[1], YAN-YU ZHANG[1], CHAO WANG[1], HAI-YONG ZHANG[2], AND YI-JUN ZHU[1]

[1]The First College of Information Engineering University, Zhengzhou, Henan 450000, China

[2]Dongguan Xinda Institute of Integrated Innovation, Dongguan, Guangdong 523000, China

Corresponding author: Chao Wang (xxgcwangchao@163.com)

This work was supported by the National Natural Science Foundation of China (NSFC) under Grant 61901524.

ABSTRACT Recently, visible light communication (VLC) in the industrial Internet of Things has been widely concerned. In these systems, multi-access technologies are always used to eliminate interference between adjacent transmitters, significantly decreasing transmission efficiency. Meanwhile, the attocell boundaries caused by multi-access technologies can also limit communication coverage and lead to frequent receiving switches. To overcome these weaknesses caused by the division of attocell, we design a boundaryless none-attocell VLC system in this paper. In the proposed system, each transmitter uses all available communication resources, and a cubic receiver is adopted to receive in both non-overlapping and overlapping areas. Specifically, we propose a scheme for adaptive signal selection, enabling the receiver to select the recoverable transmitting signals. After that, we introduce an adaptive channel estimation and signal recovery method, which adaptively achieves signal combining and overlapping signal recovery. Our simulations verify the proposed scheme and demonstrate that the proposed system with the adaptive receiving scheme has better error performance and broader communication coverage than the traditional attocell system.

INDEX TERMS Adaptive receiving, boundaryless none-attocell system, industrial Internet of Things, visible light communication.

I. INTRODUCTION

Recently, the utilization of visible light communication (VLC) in the Industrial Internet of Things (IIoT) has been widely studied because of VLC 's superior qualities, including endogenous security and high-efficiency [1]–[4]. In IIoTs, VLC transmitters are densely arranged to broadcast the status data of their covering area. The coverages of these transmitters always overlap with each other, leading to severe signal interference [5], [6]. Therefore, the concept of attocell has been introduced to overcome the interference [7], [8].

In attocell systems, multi-access technologies including frequency division multi-access (FDMA), time division multi-access, code division multi-access, etc. are always used between adjacent transmitters [9]–[14]. These technologies divide communication resources into orthogonal ones for different transmitters, and thus the communication efficiency is significantly decreased.

Meanwhile, the communication coverage is divided into several attocells without overlapping at the receiving end. However, these attocells' boundaries limit the communication coverage because the receiver could only receive from one transmitter at a time. Additionally, when the receiver moves to another attocell, handover is operated to match the new transmitter, which includes a series of control and feedback above the physical layer and could increase communication latency [15], [16].

To improve the communication efficiency and expand transmitters' coverage, we consider establishing a boundaryless VLC system removing the concept of attocell, where transmission is carried out without multi-access technologies, and adjacent transmitters' communication coverage can overlap. In this system, every transmitter transmits signals using all available communication resources without considering

The associate editor coordinating the review of this manuscript and approving it for publication was Chao Zuo.

interference. The receiver can adaptively achieve anti-noise receiving in non-overlapping areas and simultaneous recovery of two transmitting signals in overlapping areas. Additionally, handover is not required due to the cancellation of boundaries.

Consequently, the contributions of our paper are summarized as follows.

- First, we propose a boundaryless none-attocell system for IIoTs. In this system, a cubic receiver is designed for spatial channel estimation and diversity receiving from different directions [17]. We divide the signal receiving into non-overlapping and overlapping cases according to the receiver's location and then conclude both receiving cases into multi-input multi-output transmission problems.
- We propose a receiving scheme adaptive to two cases, including signal selection and recovery. For signal selection, we design a multi-subframe format and offer a method for recoverable signal recognition. For adaptive signal recovery, we apply a spatial channel estimation based on the average receiving power of the cubic receiver, which adaptively estimates the channel matrix in both cases without receiving mode switch and channel training sequence. After that, an adaptive signal recovery method is also introduced.
- Finally, we simulate the communication performance of the none-attocell transmission and adaptive receiving scheme. The results demonstrate that, because of the full-resource transmission and adaptive receiving, the boundaryless none-attocell transmission has a lower error rate and broader communication coverage than the traditional attocell system with flat receivers.

The remainder of our paper is organized as follows. First, we introduce our system model in Section II. Then, we present an adaptive signal selection and recovery scheme in Section III. After that, some simulations are conducted in Section IV. Finally, we conclude the paper in Section V.

II. BOUNDARYLESS NONE-ATTOCELL SYSTEM MODEL

In this paper, we propose a boundaryless none-attocell VLC system as Fig. 1. At the transmitting end, Lambertian transmitters are arranged on a straight line with the same interval D [18], [19]. These transmitters simultaneously broadcast signals modulated by different data using all available communication resources rather than multi-access technologies. Note that D is reasonably set to guarantee the communication and illumination coverage but not make the transmitters too intensive. A mobile user with a VLC receiver moves in transmitters' coverage at the receiving end, including non-overlapping area (Case A) and overlapping area (Case B). The receiver requires anti-noise receiving from the corresponding transmitter in Case A. In Case B, the user needs simultaneous recovery of two transmitting signals from the overlapping receiving signals for boundary cancellation. Note that to simplify the receiving process, we do not consider cases where coverage of more than two transmitters overlaps with each other. For Lambertian light sources, the light intensity far from the center of the light spot is significantly attenuated, making the above situation rarely happens. Even though there is a need for dense distribution of light sources, the mentioned situations can be avoided by adjusting the half-power angle of transmitters.

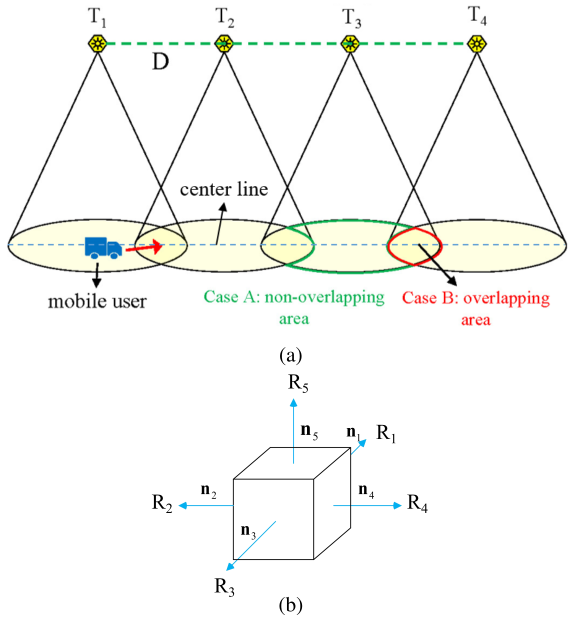

FIGURE 1. Diagram of (a) mobile VLC in IIoT scenarios and (b) cubic receiver.

In order to achieve anti-noise receiving and multiple signal recovery, we adopt a CR equipped with five photon detectors (PDs) R_i $(i = 1, 2, \ldots, 5)$ on its top and side surfaces as Fig. 1b to receive from different directions. CR's two opposite receiving surfaces have opposite normal vectors and can be used to simultaneously receive from two transmitters. The top receiving surface can receive from the nearest transmitter like the traditional flat receiver. The unique receiver structure is conducive to the completion of multi-input channel estimation and signal reception. The receiver is not rotary in moving process, keeping the normal vectors n_2 and n_4 parallel to centerline and n_5 vertical to floor.

According to CR's multiple receiving feature, we analyze and design the system under MIMO model [20], [21]. Under ideal signal sampling, the transmission follows $Y = C_s H P_t + N_0$, where Y is the vector of signal amplitudes received by five PD arrays, Cs is PD 's responsivity [22], H is channel matrix without considering reflected light, P_t is the vector of transmitting power by two transmitters, and N_0 is a zero-mean Gaussian noise vector. For ease of presentation, we convert the equation to

$$P_r = HP_t + N \tag{1}$$

where P_r is the vector of receiving power from five PDs, and N is another zero-mean Gaussian noise vector. Next, we will introduce an adaptive signal selection and recovery scheme cooperated with CR for boundaryless none-attocell model.

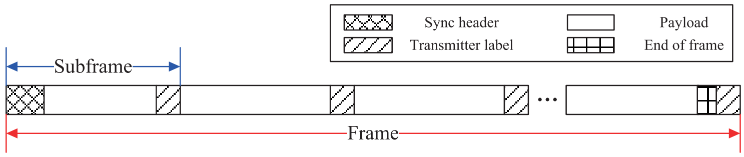

FIGURE 2. Frame structure diagram for boundryless none-attocell system.

III. ADAPTIVE SIGNAL SELECTION & RECOVERY SCHEME

The scheme of adaptive signal selection and recovery aims to achieve two functions. In signal selection, the receiver can adaptively select the transmitting signals to receive after the recoverable signals are recognized. In signal recovery, CR adaptively achieves anti-noise recovery of one transmitting signal in Case A and simultaneous recovery of two transmitting signals from overlapping signals in Case B.

A. ADAPTIVE SIGNAL SELECTION

In this part, we first design a frame format for adaptive signal selection, which enables the overlapped transmitting signals to be separable rather than multi-access technologies. Based on the frame format, we realize recoverable signal recognition by analysing signal components and CR positioning to serve the user's adaptive receiving selection.

1) FRAME FORMAT DESIGN

To adapt the channel change in the user's movement, we propose a frame format as Fig. 2. This format consists of multiple subframes of $(L_l + L_s)$ bits, which is the unit of our signal processing. A constant sync header is configured at the head of the frame to detect the start of the transmitting signal. There is a transmitter label (TL) of L_l bits at the end of each subframe, which helps to recognize the transmitters and estimate the channel. We construct all transmitter labels into a set $\mathcal{L} = \{l_T\}$, where T is the serial number of transmitters, noting that $\mathcal{L}$ is stored in each receiver. The correlation between different TLs is tiny. Additionally, an end-of-frame mark is also arranged.

2) RECOVERABLE SIGNAL RECOGNITION FOR USER 's ADAPTIVE RECEIVING SELECTION

Our main idea is that we first roughly position the user by figuring out its two adjacent transmitters T_l and T_r based on TL and then analyze the recoverable transmitting signal according to T_l, T_r and synchronization result. Hence, the user knows the recoverable transmitting signals and adaptively selects them according to their real-time location. Before we introduce the method, we define a correlation operation which is the basis of transmitter identification.

Definition 1: There is a correlation operation

$$\mathcal{R}(s_i, l_T) = \sum_{k=1}^{L_m} (2l_{T,k} - 1) \left[s_{i,\ \bmod\ (k+j, L_s)} - \frac{1}{L_s} \sum_{k=1}^{L_s} s_{i,k} \right] \tag{2}$$

where s_i is the sample vector of a subframe length received by R_i, j is the position of TL 's first bit in sampling sequence which is obtained by synchronization, and mod $(\cdot, L_s)$ denotes modular L_s arithmetic.

Now, we introduce the joint analysis of recoverable signal and user location method in three cases, noting that we operate synchronization by sliding correlation [23].

- *Case 1. Both s_2 and s_4 achieve synchronization*. If the average power of s_2 is larger than s_4, then $T_l = \max_{T_i} \mathcal{R}(s_2, l_{T_i})$ and $T_r = T_l + 1$. Otherwise, $T_r = \max_{T_i} \mathcal{R}(s_4, l_{T_i})$ and $T_l = T_r - 1$. In this case, both signals from T_l and T_r are recoverable.
- *Case 2. Only one of s_2 and s_4 achieves synchronization.* If s_2 is synchronized, then $T_l = \max_{T_i} \mathcal{R}(s_2, l_{T_i})$, $T_r = T_l + 1$ and signal transmitted by T_l is recoverable. Otherwise, $T_r = \max_{T_i} \mathcal{R}(s_4, l_{T_i})$, $T_l = T_r - 1$ and signal transmitted by T_r is recoverable.
- *Case 3. Only s_5 achieves synchronization.* First, figure out the nearest transmitter $T_0 = \max_{T_i} \mathcal{R}(s_5, l_{T_i})$, then compare $\mathcal{R}(s_2, l_{T_0})$ and $\mathcal{R}(s_4, l_{T_0})$. If $\mathcal{R}(s_2, l_{T_0}) > \mathcal{R}(s_4, l_{T_0})$, then $T_l = T_0$, $T_r = T_0 + 1$ and signal of T_l is recoverable. Otherwise, $T_r = T_0$, $T_l = T_0 - 1$ and signal of T_r is recoverable.

Since each subframe has a TL, CR can timely detect the change of transmitters and change the real-time signal selection scheme as long as a subframe is recently received, which is suitable for mobile VLC.

B. ADAPTIVE SIGNAL RECOVERY

In this part, we first propose a channel estimation method adaptive to both cases. Based on the estimated H, we offer a signal recovery method that adaptively realizes signal combining in Case A and overlapping signal recovery in Case B.

1) ADAPTIVE CHANNEL ESTIMATION

To improve the transmitting efficiency and the adaptability to users' movement, this channel estimation method uses the average power of CR's multiple receiving signals in one subframe rather than the channel training sequence [24].

The method is designed according to Lambertian radiation feature and CR 's geometrical relationship. Here, we present the geometrical diagram of Case A and Case B as Fig. 3. We calculate the mean power of receiving signals in a subframe length and denote them as $\bar{P}_r = \left[\bar{P}_1\ \bar{P}_2\ \bar{P}_3\ \bar{P}_4\ \bar{P}_5 \right]^T$,

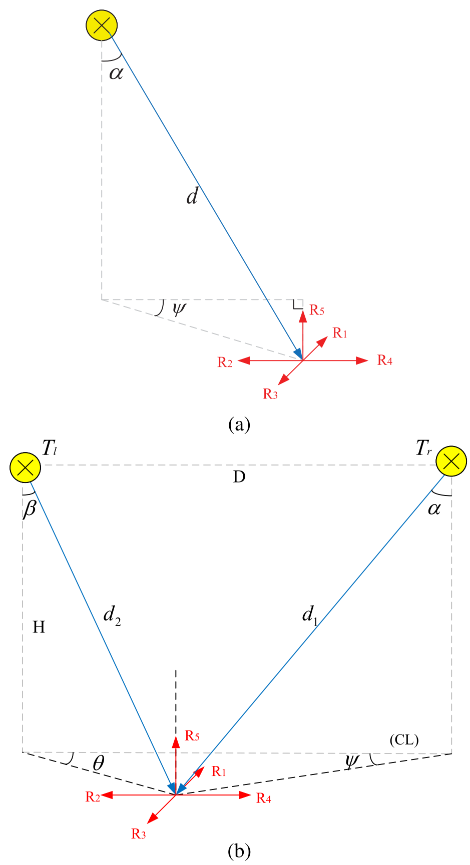

FIGURE 3. **Geometrical diagram of (a) Case A and (b) Case B.**

where $\bar{P}_i$ corresponds to R_i. Then, we can estimate channel matrix of Case B using Theorem 1.

Theorem 1: The estimated channel matrix $\hat{H}$ in Case B (Fig. 3b) satisfies

$$\hat{H} = \begin{cases} \begin{bmatrix} \hat{h}_1 \sin\hat{\alpha}\sin\hat{\psi} & \hat{h}_2 \sin\hat{\beta}\sin\hat{\theta} \\ 0 & \hat{h}_2 \sin\hat{\beta}\cos\hat{\theta} \\ 0 & 0 \\ \hat{h}_1 \sin\hat{\alpha}\cos\hat{\psi} & 0 \\ \hat{h}_1 \cos\hat{\alpha} & \hat{h}_2\cos\hat{\beta} \end{bmatrix}, & \bar{P}_1 \geq \bar{P}_3 \\ \begin{bmatrix} 0 & 0 \\ 0 & \hat{h}_2 \sin\hat{\beta}\cos\hat{\theta} \\ \hat{h}_1 \sin\hat{\alpha}\sin\hat{\psi} & \hat{h}_2 \sin\hat{\beta}\sin\hat{\theta} \\ \hat{h}_1 \sin\hat{\alpha}\cos\hat{\psi} & 0 \\ \hat{h}_1 \cos\hat{\alpha} & \hat{h}_2\cos\hat{\beta} \end{bmatrix}, & \bar{P}_1 < \bar{P}_3 \end{cases} \quad (3)$$

where $\hat{h}_1$ and $\hat{h}_2$ are the estimated channel factors between T_r, T_l and CR. Set $X_1 = \hat{h}_1 \big/ \hat{d}_1$ and $X_2 = \hat{h}_2 \big/ \hat{d}_2$, and then

$$\begin{cases} X_1 = \dfrac{\bar{P}_5 + \bar{P}_4 - \bar{P}_2 \pm \sqrt{\Delta}}{2P_0 D} \\ X_2 = \dfrac{\bar{P}_5 + \bar{P}_2 - \bar{P}_4 \mp \sqrt{\Delta}}{2P_0 D} \end{cases} \quad (4)$$

where $\Delta = \bar{P}_5^2 + \bar{P}_4^2 + \bar{P}_2^2 - 2\bar{P}_4\bar{P}_2 - 2\bar{P}_4\bar{P}_5 - 2\bar{P}_2\bar{P}_5$, and P_0 is the mean power of transmitting signals. Choose the feasible solution from two roots of X_1 and X_2 which satisfies $\left[\mathcal{R}\left(s_5, l_{T_l}\right) - \mathcal{R}\left(s_5, l_{T_r}\right)\right](X_1 - X_2) \geq 0$. Note that if T_l is not synchronized with CR, we assume that $\mathcal{R}\left(s_5, l_{T_l}\right) = 0$, and the same assumption goes for T_r. Then,

$$\hat{d}_i = \left(\frac{m_0 + 1}{2\pi X_i} A_r H^{m_0}\right)^{\frac{1}{m_0+3}}, \quad i = 1, 2 \quad (5)$$

where A_r is the detective area of PD array, and $m_0 = -\ln 2 \big/ \ln\psi_h$ (ψ_h is the half-power semi-angle of transmitters). Then, other varieties are obtained as (6).

$$\begin{cases} \hat{\alpha} = \arccos\dfrac{H}{\hat{d}_1} \\ \hat{\beta} = \arccos\dfrac{H}{\hat{d}_2} \\ \hat{h}_1 = X_1\hat{d}_1 \\ \hat{h}_2 = X_2\hat{d}_2 \\ \hat{\psi} = \arccos\dfrac{\bar{P}_4}{P_0\hat{h}_1\sin\hat{\alpha}} \\ \hat{\theta} = \arccos\dfrac{\bar{P}_2}{P_0\hat{h}_2\sin\hat{\beta}} \end{cases} \quad (6)$$

Meanwhile, Theorem 1 obeys Property 1, the proof of which is in Appendix B.

Property 1: When transmitter interval D is large enough, the channel estimation result for Case B is equal to Case A (Fig. 3a).

Therefore, our channel estimation method is adaptively suitable for any location of CR.

2) ADAPTIVE SIGNAL RECOVERY METHOD

According to the estimated channel matrix, we could achieve anti-noise and anti-interference signal recovery based on the signal combination and minimum mean square error criterion [25].

In this algorithm, we first construct all the possible combinations of two transmitters' emitting power into a set $\mathcal{X} = \{X_i\}$. After that, we determine the transmitted power combination

$$\hat{X} = \min_{X_i} \left\| P_r - \hat{H}X_i \right\| \quad (7)$$

Then, we recover the transmitted data from $\hat{X}$ according to the preset mapping relationship. For Case A, one of the data streams can be robustly recovered because of signal combining, and the other data stream is randomly determined, which would not be selected to receive due to recoverable signal analysis. For Case B, data from two adjacent transmitters are recovered simultaneously. In this way, signals are adaptively and boundaryless recovered in two cases.

IV. SIMULATION

In this section, we operate simulations to verify the communication enhancement including error rate and coverage of the

TABLE 1. Simulation setup.

Parameter	Symbol	Value
Location of transmitters	-	(-2, 0, 3) (2, 0, 3)
Transmit power	P_0	20 [W]
Semi-angle of half power	ψ_h	45 [°]
Modulation	-	Pulse amplitude modulation (PAM)
Data Rate	R_b	-
Payload length	L_s	$10^{-3}R_b$ [bit]
TL length	L_l	60 [bit]
Sync header length	-	128 [bit]
Detecting area	A_r	100 [mm^2]
PD 's responsivity [22]	C_s	0.64 [A/W]
Equivalent noise power	-	2.8×10^{-15} [W/Hz$^{0.5}$]
Number of PD	-	1×5
Receiver 's location	-	$(x, y, 0)$

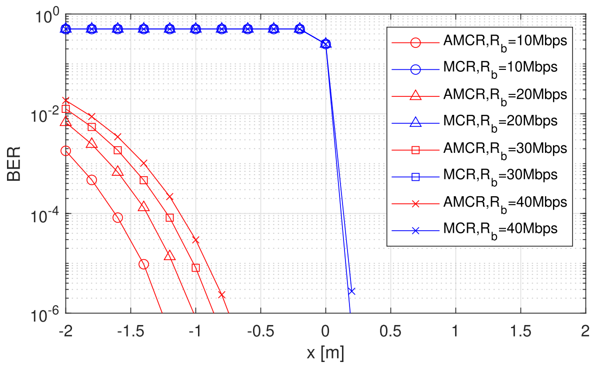

FIGURE 4. BER distribution on center line ($y = 0$) under different R_b using CR-based adaptive multi-channel receiving (AMCR) and single-channel receiving (SCR).

proposed boundaryless none-attocell system and its adaptive receiving scheme. All of these simulations are operated in the scenario as Fig. 1. The parameters of Simulation A and B are in Tab. 1.[1]

A. COMPARISON OF ADAPTIVE MULTI-CHANNEL RECEIVING & SINGLE CHANNEL RECEIVING

We compare the bit error rate (BER) when using CR-based adaptive multi-channel receiving and single-channel receiving, noting that single channel receiving uses a flat receiver with 5 PDs facing the ceiling. Here, $T_1 \sim T_4$ transmit different signals using 2-PAM without multi-access technology under different R_b.

Because of the symmetry of the system, we only present BER of receiving from T_3 when $x \in [-2, 2]$ in Fig. 4. As we can see, when the receiver is closer to T_3, the BER of both methods is very low. However, when the receiver is closer to T_2, the BER of SCR severely deteriorates, while AMCR performs far better to enable the receiving in most areas. The result illustrates that the CR-based adaptive multi-channel receiving method has broader communication coverage and can simultaneously receive from two transmitters.

[1] PD 's parameters are referenced as HAMAMATSU S12915-1010R.

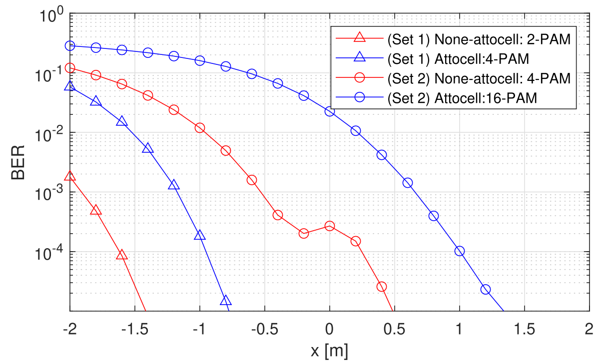

FIGURE 5. BER distribution on center line ($y = 0$) in none-attocell system and attocell system.

B. COMPARISON OF NONE-ATTOCELL SYSTEM & ATTOCELL SYSTEM

Now we compare the BER distribution in the boundaryless none-attocell system with AMCR and the attocell system with SCR, which uses FDMA between adjacent transmitters. In the attocell system, every transmitter only uses half of the available bandwidth, and adjacent transmitters use different frequency bands to cancel interference [26], [27]. We operate two sets of simulations. In each set, the total available bandwidths of two systems are the same, and two systems use different PAM orders to make $R_b = 10$Mbps.

As shown in Fig. 5, BER does not steeply change at $x = 0$ for both systems, indicating that both multi-access technology and none-attocell design expand the communication coverage. However, in both simulation sets, the none-attocell system has a lower error rate at the same receiver's location compared with the attocell system which uses frequency multiplexing technology. Although for the 4-PAM none-attocell system, BER fluctuates around $x = 0$ because of the wrong choice of feasible solutions for X_1 and X_2, the effect is not significant since their difference is slight. Therefore, the proposed system could achieve broader communication coverage for each transmitter due to the full utilization of frequency bandwidth.

C. COVERAGE IMPROVEMENT OF BOUNDARYLESS NONE-ATTOCELL SYSTEM

Next, we compare the communication coverage of the none-attocell system and attocell system. Here, we adjust the value of ψ_h to control the degree of signal interference. Three transmitters are located at (−8,0,3), (−4,0,3), (0,0,3), (4,0,3) and (8,0,3). We test the BER distribution on the floor for the center transmitter. The contour maps of BER are as Fig. 6, where the dashed line means the non-attocell system with 2-PAM and the full line represents the attocell system with 4-PAM. The different colored lines respectively are BER equal to 1×10^{-2}, 1×10^{-3} and 1×10^{-4}.

For the simulated ψ_h, it is obvious that the proposed scheme has broader communication coverage than the attocell system with FDMA. Meanwhile, as the interference

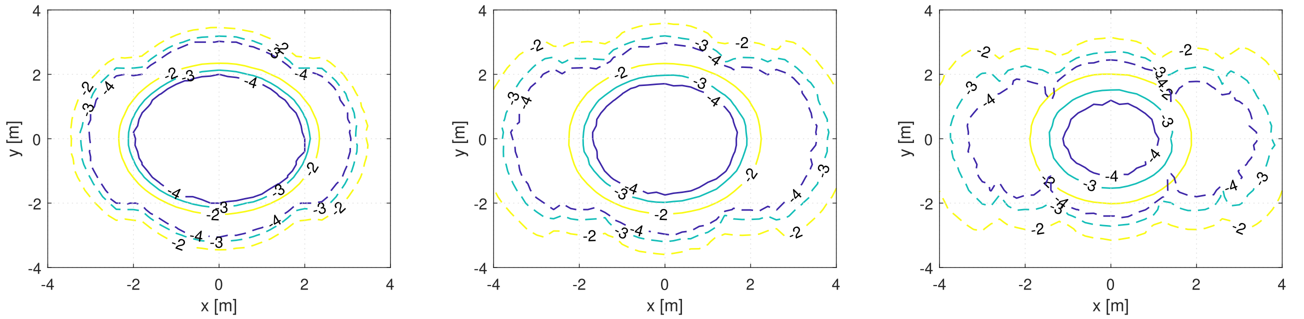

(a) (b) (c)

FIGURE 6. Top view of communication coverage in boundaryless none-attocell system and attocell system under (a) $\psi_h = 30°$ (b) $\psi_h = 45°$ and (c) $\psi_h = 60°$.

increases, i.e. ψ_h becomes larger, the coverage enhancement improves. This is because the proposed scheme can adaptively recover signals in the same frequency band even if they are overlapped, while the attocell system cannot. Consequently, our non-attocell system achieves broader communication coverage for each transmitter under interference, making it more adaptable to mobile users and providing more possibilities for the light source arrangement in IIoTs.

V. CONCLUSION

In this paper, we designed a boundaryless none-attocell VLC system for IIoT. In this system, every transmitter transmits without multi-access technology. A CR with adaptive receiving scheme boundaryless receives from one transmitter in non-overlapping areas or two transmitters in overlapping areas. Our simulations verified the BER decrease of adaptive boundaryless receiving and none-attocell transmission and demonstrated that our system has broader communication coverage.

APPENDIX A
PROOF OF THEOREM 1

In Fig. 3b, the geometrical relationship in (8) works.

$$\begin{cases} \cos\alpha = H/d_1 \\ \cos\beta = H/d_2 \\ d_1 \sin\alpha \sin\psi = d_2 \sin\beta \sin\theta \\ d_1 \sin\alpha \cos\psi + d_2 \sin\beta \cos\theta = D \end{cases} \tag{8}$$

where D and H are known. Taking the expectation of (1), then

$$EP_r = \left[EP_1 \ \ EP_2 \ \ EP_3 \ \ EP_4 \ \ EP_5 \right]^T = H\left(P_0 1^T\right) \tag{9}$$

where EP_r is the expectation of P_r. Here, we substitute EP_i by $\bar{P}_i$. Then, (4) can be acquired with (8), (9) and (3). After that, because X_1, X_2 and $\mathcal{R}(s_5, l_T)$ are both negatively correlated with d, so $\left[\mathcal{R}\left(s_5, l_{T_l}\right) - \mathcal{R}\left(s_5, l_{T_r}\right)\right](X_1 - X_2) \geq 0$. Thus, the feasible X_1 and X_2 are obtained. Moreover, (5) is based on Lambertian model, and (6) is then acquired.

APPENDIX B
PROOF OF PROPERTY 1

For the case in Fig. 3a, there is $EP_5 = P_0 h \cos\alpha$, $P_a = P_0 h \sin\alpha \sin\psi$ and $P_b = P_0 h \sin\alpha \cos\psi$, where h is the channel factor, $P_a = \max\{EP_1, EP_3\}$, and $P_b = \max\{EP_2, EP_4\}$. Similarly, we substitute EP_i using $\bar{P}_i$, and then $\hat{h} = \bar{P}_5 / (P_0 \cos\hat{\alpha})$, $\hat{\alpha} = acos\left(\sqrt{P_a^2 + P_b^2} \Big/ \bar{P}_5\right)$ and $\hat{\psi} = atan\left(P_a/P_b\right)$. Thus, the estimated channel of Case A is

$$\hat{H} = \left[\hbar_1 \ \ \hbar_2 \ \ \hbar_3 \ \ \hbar_4 \ \ h\cos\alpha \right]^T \tag{10}$$

Here, $\hbar_1 = \hat{h}\sin\hat{\alpha}\sin\hat{\psi}$ and $\hbar_3 = 0$ for $\bar{P}_1 \geq \bar{P}_3$. Otherwise, $\hbar_1 = 0$ and $\hbar_3 = \hat{h}\sin\hat{\alpha}\sin\hat{\psi}$. Additionally, when $\bar{P}_2 \geq \bar{P}_4$, $\hbar_2 = \hat{h}\sin\hat{\alpha}\cos\hat{\psi}$ and $\hbar_4 = 0$, or else $\hbar_2 = 0$ and $\hbar_4 = h\sin\alpha\cos\psi$. If we take $T_i\,(i = l, r)$ infinitely distant from CR, then $D \to +\infty$ and $h_i \to 0$. Thus, the estimation model for Case B transfers to that of Case A, and elements in ith column turn into '0's. Hence, *Property 1* is proved.

REFERENCES

[1] F. Delgado-Rajo, A. Melian-Segura, V. Guerra, R. Perez-Jimenez, and D. Sanchez-Rodriguez, "Hybrid RF/VLC network architecture for the Internet of Things," *Sensors*, vol. 20, no. 2, p. 478, Jan. 2020.

[2] M. Durgun and L. Gokrem, "VLC4WoT: Visible light communication for web of things," *KSII Trans. Internet Inf. Syst.*, vol. 14, no. 4, pp. 1502–1519, 2020.

[3] H. Yang, A. Alphones, W. Zhong, C. Chen, and X. Xie, "Learning-based energy-efficient resource management by heterogeneous RF/VLC for ultra-reliable low-latency industrial IoT networks," *IEEE Trans. Ind. Informat.*, vol. 16, no. 8, pp. 5565–5576, Aug. 2020.

[4] M. Jani, P. Garg, and A. Gupta, "On the performance of a cooperative PLC-VLC indoor broadcasting system consisting of mobile user nodes for IoT networks," *IEEE Trans. Broadcast.*, vol. 67, no. 1, pp. 289–298, Mar. 2021.

[5] J. Chen, Z. Wang, and R. Jiang, "Downlink interference management in cell-free VLC network," *IEEE Trans. Veh. Technol.*, vol. 68, no. 9, pp. 9007–9017, Sep. 2019.

[6] H. B. Eldeeb, H. A. I. Selmy, H. M. Elsayed, and R. I. Badr, "Interference mitigation and capacity enhancement using constraint field of view ADR in downlink VLC channel," *IET Commun.*, vol. 12, no. 16, pp. 1968–1978, Oct. 2018.

[7] J. Beysens, Q. Wang, and S. Pollin, "Increasing throughput of dense-transmitter VLC networks through adaptive distributed MISO," in *Proc. IEEE Int. Conf. Commun. (ICC)*, May 2018, pp. 1–6.

[8] C. Chen, D. A. Basnayaka, and H. Haas, "Downlink performance of optical attocell networks," *J. Lightw. Technol.*, vol. 34, no. 1, pp. 137–156, Jan. 1, 2016.

[9] Z. Li and C. Zhang, "An improved FD-DFE structure for downlink VLC systems based on SC-FDMA," *IEEE Commun. Lett.*, vol. 22, no. 4, pp. 736–739, Jan. 2018.

[10] A. W. Azim, Y. Le Guennec, and G. Maury, "Hermitian symmetry free optical-single-carrier frequency division multiple access for visible light communication," *Opt. Commun.*, vol. 415, pp. 177–185, May 2018.

[11] D.-F. Zhang, H.-Y. Yu, and Y.-J. Zhu, "A multi-user joint constellation design of color-shift keying for VLC downlink broadcast channels," *Opt. Commun.*, vol. 473, Oct. 2020, Art. no. 126001.

[12] Y. Guo, K. Xiong, Y. Lu, D. Wang, P. Fan, and K. B. Letaief, "Achievable information rate in hybrid VLC-RF networks with lighting energy harvesting," *IEEE Trans. Commun.*, vol. 69, no. 10, pp. 6852–6864, Oct. 2021.

[13] Y. Qiu, S. Chen, H.-H. Chen, and W. Meng, "Visible light communications based on CDMA technology," *IEEE Wireless Commun.*, vol. 25, no. 2, pp. 178–185, Apr. 2017.

[14] D. Chen, J. Wang, H. Lu, L. Feng, and J. Jin, "Experimental demonstration of quasi-synchronous CDMA-VLC systems employing a new OZCZ code construction," *Opt. Exp.*, vol. 27, no. 9, pp. 12945–12956, 2019.

[15] M. S. Demir, H. B. Eldeeb, and M. Uysal, "CoMP-based dynamic handover for vehicular VLC networks," *IEEE Commun. Lett.*, vol. 24, no. 9, pp. 2024–2028, Sep. 2020.

[16] A. M. Vegni and T. D. C. Little, "Handover in VLC systems with cooperating mobile devices," in *Proc. Int. Conf. Comput., Netw. Commun. (ICNC)*, Jan. 2012, pp. 126–130.

[17] P. Nabavi and M. Yuksel, "Comprehensive design and prototype of VLC receivers with large detection areas," *J. Lightw. Technol.*, vol. 38, no. 16, pp. 4187–4204, Aug. 15, 2020.

[18] H. Chen and Z. Xu, "OLED panel radiation pattern and its impact on VLC channel characteristics," *IEEE Photon. J.*, vol. 10, no. 2, pp. 1–10, Apr. 2017.

[19] Y. S. Eroglu, Y. Yapici, and I. Güvenc, "Impact of random receiver orientation on visible light communications channel," *IEEE Trans. Commun.*, vol. 67, no. 2, pp. 1313–1325, Feb. 2018.

[20] O. I. Younus, H. Le Minh, P. T. Dat, N. Yamamoto, A. T. Pham, and Z. Ghassemlooy, "Dynamic physical-layer secured link in a mobile MIMO VLC system," *IEEE Photon. J.*, vol. 12, no. 3, pp. 1–15, Apr. 2020.

[21] Y.-Y. Zhang, "Intrinsic robustness of MISO visible light communications: Partial CSIT can be as useful as perfect one," *IEEE Trans. Commun.*, vol. 67, no. 2, pp. 1297–1312, Feb. 2018.

[22] B. G. Guzman, A. L. Serrano, and V. P. G. Jimenez, "Cooperative optical wireless transmission for improving performance in indoor scenarios for visible light communications," *IEEE Trans. Consum. Electron.*, vol. 61, no. 4, pp. 393–401, Jan. 2015.

[23] J.-C. Lin, "Noncoherent sequential PN code acquisition using sliding correlation for chip-asynchronous direct-sequence spread-spectrum communications," *IEEE Trans. Commun.*, vol. 50, no. 4, pp. 664–676, Apr. 2002.

[24] J.-B. Wang, Y. Jiao, X.-Y. Dang, M. Chen, X.-X. Xie, and L.-L. Cao, "Training sequence based channel estimation for indoor visible light communication system," *Optoelectronics Lett.*, vol. 7, no. 3, pp. 213–216, May 2011.

[25] H. Y. Zhu, Y. J. Zhu, J. K. Zhang, and Y. Y. Zhang, "A double-layer VLC system with low-complexity ML detection and binary constellation designs," *IEEE Commun. Lett.*, vol. 19, no. 4, pp. 561–564, Apr. 2015.

[26] E. A. Jarchlo, S. M. Kouhini, H. Doroud, G. Maierbacher, M. Jung, B. Siessegger, Z. Ghassemlooy, A. Zubow, and G. Caire, "Flight: A flexible light communications network architecture for indoor environments," in *Proc. 15th Int. Conf. Telecommun. (ConTEL)*, Jul. 2019, pp. 1–6.

[27] E. Dinc, O. Ergul, and O. B. Akan, "Soft handover in OFDMA based visible light communication networks," in *Proc. IEEE 82nd Veh. Technol. Conf. (VTC-Fall)*, Sep. 2015, pp. 1–5.

JING-SHU XUE received the B.S. degree from Information Engineering University, Zhengzhou, Henan, China, in 2019, where she is currently pursuing the M.S. degree. Her main research interests include wireless communication theory, visible light communications, and signal processing.

YAN-YU ZHANG received the B.S. degree in communication engineering, the M.S. degree in communication and information system, and the Ph.D. degree in information and communication engineering from Information Engineering University, Zhengzhou, China, in 2009, 2012, and 2016, respectively. He is currently a Lecturer with Information Engineering University. His research interests include finite-alphabet signal processing for radio frequencies, optical wireless communications, funda-mental structure establishment, and energy-efficient designs for multiuser finite-alphabet signals.

CHAO WANG received the B.S. degree in communication engineering from Tianjin University, in 2011, and the M.S. and Ph.D. degrees in information system engineering from Information Engineering University, Zhengzhou, China, in 2014 and 2018, respectively. He is currently a Lecturer with Information Engineering University. His research interests include optical wireless communications and signal processing.

HAI-YONG ZHANG received the master's degree from Information Engineering University, Zhengzhou, Henan, China, in 2017. He is currently working with the Dongguan Xinda Institute of Integrated Innovation, Dongguan, Guangdong, China. His main research interests include wireless communication theory and visible light communications.

YI-JUN ZHU received the B.Eng., M.Sc., and Ph.D. degrees from Information Engineering University, Zhengzhou, Henan, China, in 1999, 2002, and 2010, respectively. In 2011, he visited at the Department of Electrical and Computer Engineering, McMaster University. He is currently with Information Engineering University. His main research interests include wireless communication theory, visible light communications, and signal processing.